Beneficial effect of in-situ citrate-grafting of hydroxyapatite surface for water treatment

D. Bouazzi, A. Mehri, K. Kaaroud, H. Touati, F. Karouia, J.M. Clacens, A. Laghzizil, B. Badraoui

Beneficial effect of in-situ citrate-grafting of hydroxyapatite surface for water treatment

D. Bouazzi[1], A. Mehri[1], K. Kaaroud[1], H. Touati[2], F. Karouia[3], J. M. Clacens[2], A. Laghzizil[4*], B. Badraoui[1]

[1]U.R. Matériaux et synthèse organique UR17ES31, Institut Préparatoire aux Etudes d'Ingénieur de Monastir, Université de Monastir, 5019 Monastir, Tunisia

[2]Institut de Chimie des Milieux et Matériaux de Poitiers, UMR 7285 Université de Poitiers-CNRS, 4, Rue Michel Brunet, BP633, 86022 Poitiers Cedex, France.

[3]Blue Marble Space Institute of Science, Exobiology Branch, NASA Ames Research Center, Moffett Field, CA 94035, USA

[4]Laboratory of Applied Chemistry of Materials, Faculty of Science, Mohammed V University in Rabat, Avenue Ibn Batouta BP.1014, Rabat Morocco.

Abstract

Hybrid materials based on hydroxyapatite (HAP) were synthesized by the co-precipitation method in the presence of citric acid (Cit) at different molar ratios Cit/HAP (wCit-HAP). By increasing the quantity of citric acid added, a loss of crystallinity of the grafted materials is observed and this grafting makes it possible to control the size of their nanoparticles and the surface characteristics. Their surface properties were tested by adsorption of methylene blue (MB) as a model dye. Several parameters influencing pollutant removal from aqueous solutions are discussed. The contact time to reach equilibrium for maximum adsorption does not exceed 60 min and the kinetic data are well fitted by a pseudo second order model. The best adsorption capacity was obtained for 0.2Cit-HAP. The calculated thermodynamic parameters showed that the adsorption was a spontaneous and endothermic process and that all $\Delta H°$ values are below 20 kJ mol^{-1}. This indicates that there are weak electrostatic Van der Waals forces as well as the formation of hydrogen bonds. This approach was proven by quantum chemical calculations performed using the density function theory (DFT) method which provided new insights into the mechanism of adsorption.

Keywords: Citrate-grafted hydroxyapatite, Surface properties, Adsorption, DFT calculation.

* Corresponding Author. Email : laghzizi@fsr.ac.ma (A. LAGHZIZIL)

1. Introduction

The assessment and management of the risk due to the presence of chemical contaminants in ecosystems is an approach that requires effective approaches integrating different skills in the field of the environment [1-3]. Toxic species resulting from any human activity (urban, industrial, agricultural, etc.) are likely to contaminate the environment in the short or medium term, and are responsible for various alterations to the environment [4, 5]. Thus, the problem of water pollution is today very worrying for emerging countries [6, 7].

Different porous solids are currently used or in the development phase to stabilize waste from various origins [8, 9]. Among them, hydroxyapatites have structural, adsorption and ion exchange properties that can contribute to their valorization [11-13]. There are important minerals in the field of biology and chemistry, which can be used as biomaterials and adsorbents. Their solubility and the surface functional groups are in particular the main factors of the retention of the chemical species. Nevertheless, their adsorption capacity is limited by the number of sites available for adsorption process [10, 14, 15]. For this, the possibility of modifying the surface of these materials by organic molecules has been widely described, reflecting the versatility of derived apatite materials. In hybrid materials, their inorganic components provide characteristics of thermal stability, structural, mechanical while the grafted organic matter changes the organofunctionalizations of the solid such as hydrophilicity, hydrophobicity, reactivity and modification of textural properties. This surface functionalization undoubtedly brings positive effects on the remediation of most toxic substances in waters despite the fact that they are widely demonstrated in the literature [16, 17]. From a well-ordered surface, the grafted molecules form covalent or pseudo-covalent bonds with the constituent ions of the apatitic surface. This grafting must be evenly distributed while preserving the apatitic structure. Indeed, hydroxyapatite has hydrogenated active sites and charges on its surface from amphoteric ≡Ca-OH and/or ≡P-OH sites capable to react with organic additives to form hybrid material. The grafting can be carried out in two (i) post-grafting on a preformed apatite surface and (ii) in-situ grafting by adding the multifunctional organic functions to the solution of mineral precursors. The first approach has been used for the incorporation of organophosphates [18, 19]. Other work has been carried out on the grafting of vinyl phosphonic acid (VPA) within the HAP matrix [20]. In situ grafting has been studied by several authors using C-POH phosphonates [21, 22], and N-C-POH aminophosphonates, gelatin [23], alginate [24, 25] on the surface of apatites [26]. The advantage of this last approach can modify both the size and the surface properties of the apatite particles and therefore the porosity of the material obtained.

Another strategy simultaneously associates surface functionalization and control of apatite structure by chelation of Ca^{2+} ions [11]. In this context, carboxylic acids appear as the most promising surface modifiers due to their strong affinity for the complexation of Ca^{2+} ions leading to inhibition of apatite crystal growth and have a good chemical affinity with biological species [27-29]. It should be remembered that the majority of studies carried out on carboxylate modified hydroxyapatite are oriented towards the biological aspect. Moreover, these functionalized materials can be good adsorbents for the majority of pollutants in water.

As presented, these features illustrate the great versatility of hybrid hydroxyapatites; in particular, the present study explores the synthesis and characterization of a series of inorganic-organic hybrid materials resulting from the reactions of hydroxyapatite and citrates at varying rates. The adsorptive properties of these organostructured hydroxyapatites in the removal of methylene blue (MB) as a model for dyes are compared to those of the pure hydroxyapatite knowing that, to our knowledge, no study has been carried out in this context. By introducing citrates rich in carboxylate functions within the hydroxyapatite matrix, it is possible to derive a good efficacy to bind MB molecules. Various experimental parameters having effects on the adsorption process are discussed (dye concentration, pH, contact time, adsorbent dose, and temperature) and have been studied in batch experiments. The kinetics, isotherms and thermodynamics of MB dye interactions with the developed adsorbents were discussed. Insights of the adsorption mechanism of methylene blue on the citrate-gradfted hydroxyapatite, a phenomenological modeling and DFT calculations have also been established by investigating the main functional groups responsible for MB adsorption.

2. Experimental

2.1. Synthesis of citrate-hydroxyapatite (Cit-HAP)

The pure hydroxyapatite (HAP) was prepared by a chemical wet method. Under nitrogen flux, 1.67 moles of Ca $(NO_3)_2.4H_2O$ (99% purity, Sigma-Aldrich) and 1 mole of $(NH_4)_2HPO_4$ (99% purity, Fluka) were independently dissolved in deionized water at room temperature. The solution containing calcium was added dropwise to that containing phosphate which was adjusted to pH 11 by addition of ammonia (25%, Prolabo). The mixture was stirred and heated under reflux at 80°C for 3 hours. After cooling with continuous stirring, the final suspensions were filtered and thoroughly washed with deionized water. The recovered precipitate (HAP) was dried overnight at 100°C in an oven. The citrate-modified hydroxyapatites (Cit-HAP) were obtained by a similar procedure to that of pure HAP, except for the calcium-containing solution which was prepared by adding a variable amount of citric

acid (99% purity, Sigma-Aldrich) to $Ca(NO_3)_2$ left under agitation during one hour before its addition to the phosphate solution to better promote the Ca^{2+}-Citrate complexation reaction and subsequently slow down the precipitation with the phosphates. According to the molar ratio w= n_{citric}/n_{Ca}^{2+} (0, 0.2, 0.4, 0.8), the resulting powders were termed w-Cit-HAP.

2.2. Techniques

The resulting solids were characterized using X-ray powder diffraction (XRD) (PANalytical X'Pert PRO powder diffractometer equipped with a fast X'Celerator detector and $Cu_{K\alpha}$ radiation). ATR FT-IR spectra were recorded on a Spectrum Two 104462 IR spectrometer using a diamond/ZnSe ATR crystal. Thermogravimetry (TG) was carried out in airflow using a SDT Q600 (TA instruments) apparatus and the thermal measurements were conducted from 25°C to 1000°C with 10°C min^{-1} as heating rate. Chemical analyses were performed by ICP-OES on a Horiba Jobin Yvon modele activa. Scanning electron microscopy (SEM) images were taken on the Hitachi S-3400N apparatus Nitrogen adsorption/desorption isotherms were recorded at 77 K using a Micromeritics TriStar. The specific surface areas (S_{BET}) were calculated according to the Brunauer-Emmet-Teller (BET) method whereas the porous volume (V_p) and pore size (D_p) distribution were estimated using the Barret-Joyner-Halenda (BJH) approximation.

2.3. Adsorption experiments

Adsorption experiments were carried out in a series of 250 mL Erlenmeyer flasks containing a given mass of adsorbent varied from 0.01 to 0.1 g and 100 mL of MB solution with different initial concentrations (20-200 mg L^{-1}). The equilibrium time was determined by preliminary kinetic measurements. The solution pH was then adjusted than 6 by addition of 0.1 M HCl or 1M NaOH solutions. After centrifugation, the supernatant liquid phase was separated and the residual MB concentration was determined by UV-visible spectroscopy at λ = 662 nm using a Bk-uv1900/bk-v1900 scanning spectrophotometer. The amount of MB adsorbed, q_e, was calculated as: $q_e=V.(C_0-C_e)/m$ (Eq.1**),** where C_0 and C_t are the MB concentration (mg L^{-1}) before and after adsorption, respectively. V is the volume of the solution (L) and m is the mass of adsorbent (g). The adsorption process of methylene blue (MB) on wCit-HAP-grafted materials was studied by modifying various parameters, namely adsorption dose (20-500 mg), MB-adsorbent contact time, pH solution (4.0 - 12.0), temperature (298-323 K), and initial dye concentration (10–200 ppm). Each test was repeated in triplicate and averaged in order to

obtain statistically valid results. Various kinetic and isotherm models were applied to fit the experimental data.

The use of NaOH for the regeneration of wCit-HAp adsorbents is a well-established method due to its high alkalinity and ability to desorb cationic dyes from the negative adsorbent surface such as hydroxyapatite and its hybrid materials. Therefore, NaOH is a very effective desorbent for methylene blue as demonstrated elsewhere [30]. After adsorption test, the different adsorbents loaded by BM dye were recovered, washed with deionized water to remove any unabsorbed dye molecules. Then, the adsorbents are kept stirred with 50 mL of a 3 mol L^{-1} NaOH solution at 298 K for 3 hours. Finally, they were washed with deionized water and dried at 80°C and used for the next cycle adsorption of BM. After adsorption test, the different adsorbents (HAP and wCit-HAP) loaded by BM dye were recovered, washed with deionized water to remove any unabsorbed dye molecules.

2.4. Theoretical approach

Theoretical reactivity parameters including E_{HOMO} the highest occupied molecular orbital energy is usually related to the ability of a molecule to lose electrons [31, 32] and E_{LUMO}, the lowest unoccupied molecular orbital energy, indicates the capacity of the molecule to accept electrons and it is associated to electron affinity, chemical hardness (η), the electronic chemical potential (μ) and energy gap (ΔE_{gap}) were calculated for methylene blue and adsorbent to evaluate their reactivity by using DFT. In addition, theoretical calculation realized with density function theory DFT/B3LYP method implanted in the GAUSSIAN (09) program [33, 34], and 6-31G (d, p) basis set were successfully used to correlate the experimental results. These parameters were calculated as follows:

$\Delta E_{gap} = E_{LUMO}-E_{HOMO}$; $\eta = ½ (E_{LUMO}-E_{HOMO})$; $\mu = -½ (E_{LUMO}+E_{HOMO})$

$\chi = -\mu$ $\sigma = 1/\eta$ $\omega = \mu^2/2\eta$ $\Delta N_{max} = -\mu/\eta$.

3. Results and discussion

3.1. Characterization of samples

XRD patterns of HAP and wCit-HAP materials are given in **Figure 1**, illustrating characteristic peaks of apatite structure without any secondary phase. By increasing the quantity of citric acid added, a loss of crystallinity is observed, indicating a decrease in the size of the crystallites estimated by the Scherer formula [35]: $D_{hkl} = K\lambda/\beta_{1/2}\cos\theta$, where θ is the diffraction angle, λ the wavelength, K is a constant depending on the crystal (0.89 for apatite crystallites) and $\beta_{½}$ is full width at half maximum (FWHM). The crystallinity (χ_c) is

calculated using an empirical relation as: $\chi_c = \sqrt[3]{\frac{K_A}{\beta_{1/2}}}$, where K_A is a constant (K_A=0.24) and β½ is the FWHM of the (002) reflection. The obtained values are reported in **Table 1**.

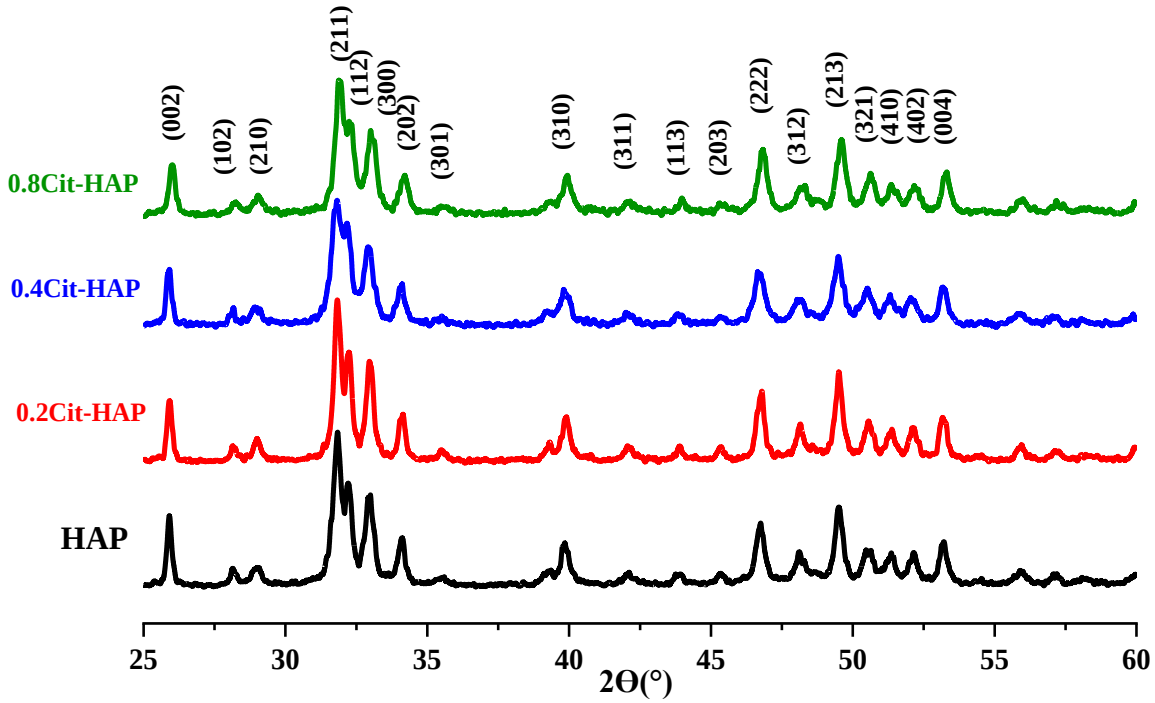

Figure 1. X-ray diffractograms of the wCit-HAP (x=0, 0.2, 0.4, 0.8).

Table 1. Particle size, parameters and crystallinity for HAP and wCit-HAP

	$\beta_{1/2}$ (002)	$D_{(002)}$ (Å)	$\beta_{1/2}$ (310)	$D_{(310)}$ (Å)	χ_C
HAP	0.212	383	0.391	216	1.437
0.2Cit-HAP	0.215	379	0.395	214	1.385
0.4 Cit-HAP	0.232	350	0.430	206	1.095
0.8 Cit-HAP	0.272	299	0.433	205	0.680

Note that the diffraction lines become broad when citric acid content is high offering a significant reduction in crystallinity compared to that of the HAP. This suggests a preferential interaction of the citrate (COO^-) groups with Ca^{2+} ions of HAP such as demonstrated elsewhere [36]. This structural change is explained by the complexation of Ca^{2+} ions by citrates which are more favorable than for the other carboxylic acids [37, 10].

Infrared spectra of the grafted materials are shown in **Figure 2**. For pure HAP, sharp peaks at ca. 1090, 1033, 960, 605, 565 and 470 cm^{-1} are attributed to PO_4 vibrations while the bands of

very low vibratory intensities around 3563 cm^{-1} and 630 cm^{-1} are attributed to OH groups. Other bands in the 1400-1450 cm^{-1} range correspond to carbonate groups, which could come from the dissolution of the surrounding CO_2 during an aqueous precipitation. Their relative intensities decrease as a function of acid citric content. In the presence of citric acid, additional bands at 1380 cm^{-1} and 1610 cm^{-1} relating to the vibrations of citrates (COO^-) around 1380 cm^{-1} and 1610 cm^{-1}, but they are located in the same range of carbonaceous vibrations (CO_3^{2-}). Another vibrational band around 1720 cm^{-1} of citric acid and that of hydroxyl OH at 3265 cm^{-1} are not detected here or of very low intensity showing that the three -COOH functions of citric acid have been deprotonated during their functionalization on the HAP matrix [11]. This result is in agreement with the hypothesis of an important interaction of the carboxylic functions of citric acid with the HAP surface.

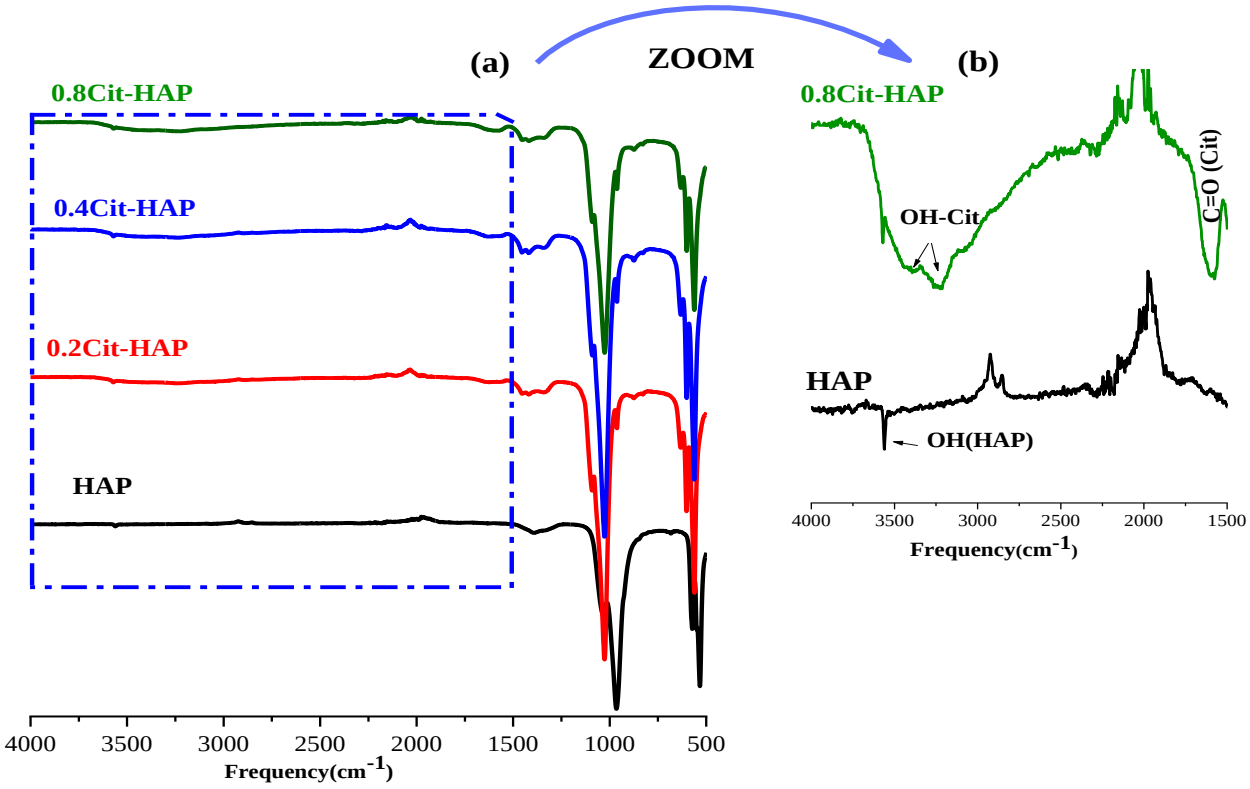

Figure 2. IR spectra of pure and citrate-modified apatites.

The thermal stability of the materials was studied by TG analysis (**Figure 3**). All materials have similar profiles with a first step in the range 25- 200°C corresponding to the desorption of water, and a second step between 200- 800°C related to the decomposition of organic matter embedded in layered hydroxyapatite. In this last step, weight loss increases with graft content, this is consistent with the increase in total organic carbon determined by the CHONS elemental microanalysis technique. The molar Ca/P ratio of the citrate-modified hydroxyapatite materials varies from 1.63 to 1.66 (**Table 2**). It should be noted that the Ca/P

molar ratio of wCit-HAP is lower than that of HAP (Ca/P=1.66). This variation is linked to the reactivity of the carboxylic acid with the constituent ions of apatite, mainly Ca^{2+} ions, which complex COO^- groups before reacting with the phosphate precursor. This is consistent with the formation of hybrid apatite materials.

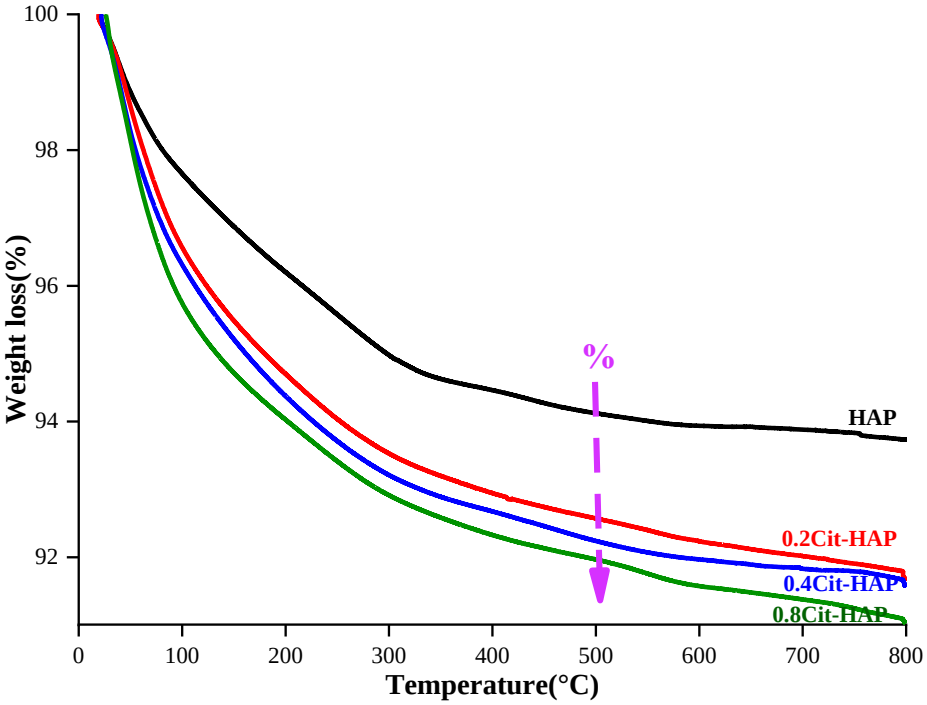

Figure 3. TG curves of pure and citrate-grafted apatites.

Table 2. Chemical composition of porous citrate-modified HAP: organic matter (%org.) Total organic carbon (%C), specific surface area S_{BET}, porous volume V_p, pore size D_p and C_{BET} constant.

	Ca/P[a]	%org[b]	%C[c]	S_{BET}/m^2g^{-1}	V_p/cm^3g^{-1}	D_p/nm	C_{BET}
HAP	1.66	2.40	0.12	57	0.31	24.5	316
0.2Cit-HAP	1.65	2.70	1.24	71	0.38	23.8	287
0.4Cit-HAP	1.64	2.90	1.59	90	0.43	21.1	257
0.8Cit-HAP	1.63	3.10	1.93	103	0.48	15.3	301

[a] From ICP-OES, [b]from TG analysis in the 200-600°C range, [c] from CHONS analysis, [d] from N_2-isothrms using BET model, [e] from N_2-isotherms using BJH model.

The N_2 adsorption-desorption isotherms of all powders dried at 100°C are illustrated in **Figure 4**. The mesoporosity of the surface of the studied materials was confirmed by the presence of hysteresis. The specific surface area increases from 57 $m^2.g^{-1}$ for the pure HAP to 103 $m^2.g^{-1}$ for 0.8Cit-HAP while V_p also increases with the content of citric acid grafted; in contrast D_p decreases (**Table 2**). The higher values of C_{BET} after citrate-grafting are indicative of the affinity of the grafted material surface for the adsorption gas and also confirm the change in texture as a function of grafting rate.

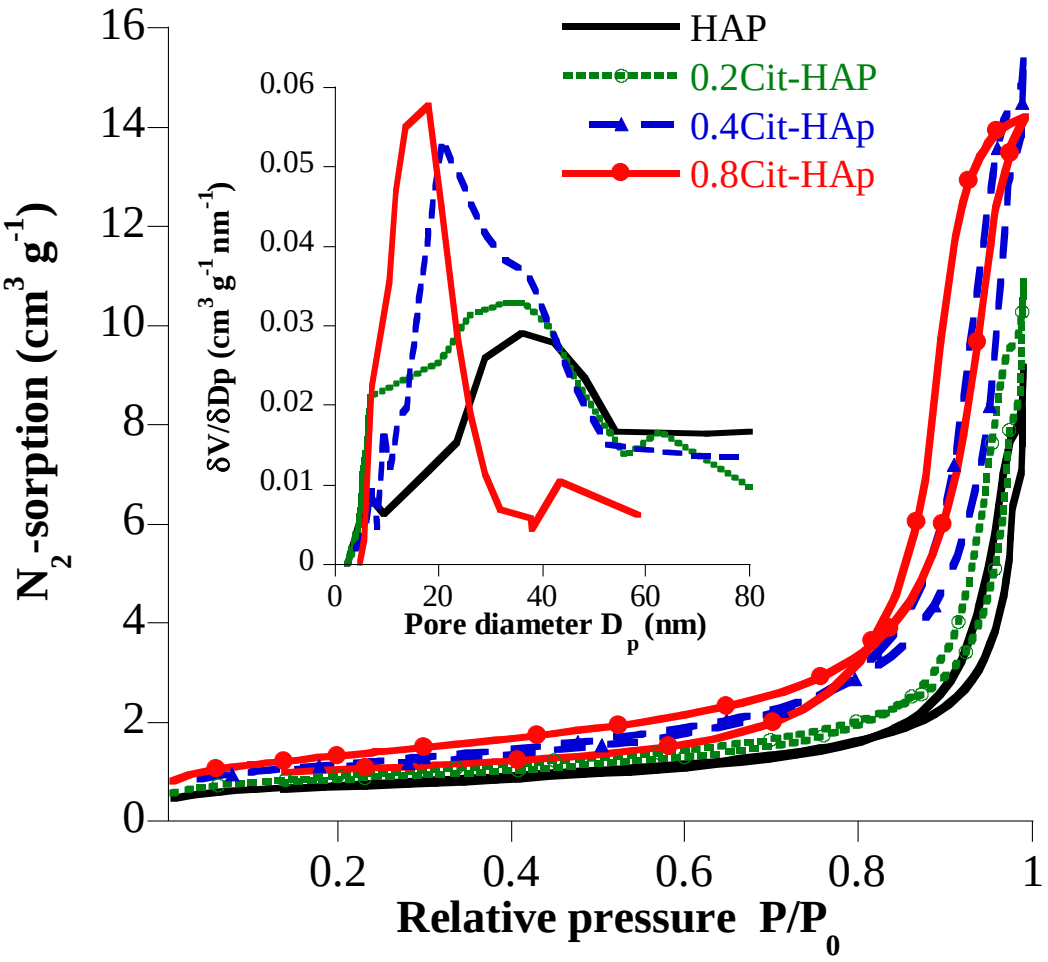

Figure 4. Nitrogen adsorption/desorption isotherms (77 K) and pore size distribution for dried powders

The Cit-grafted HAP powders were difficult to observe by SEM due to the presence of organic matter (**Fig. 5**). All the samples consist mainly of granules without relief with micrometric plates sometimes visible.

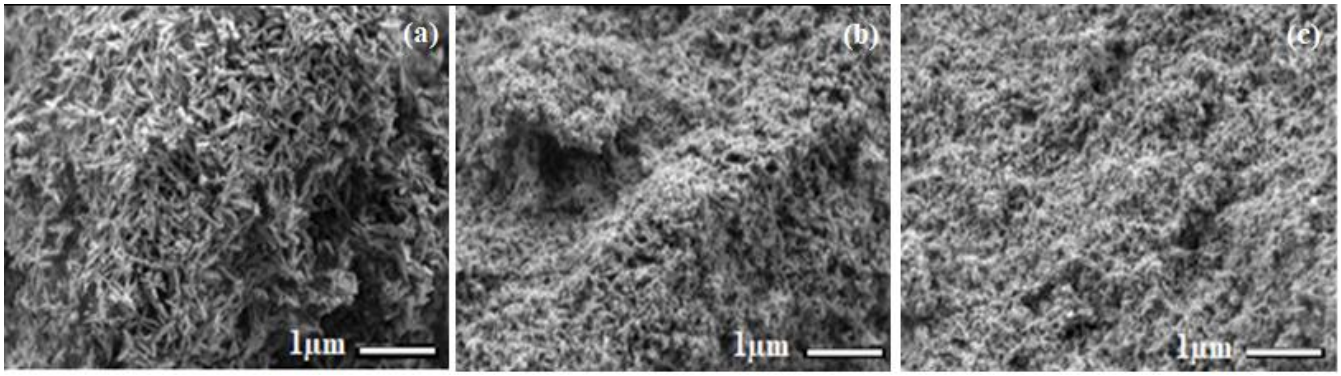

Figure 5. SEM images of (a) HAP, (b) 0.4Cit-HAP and (c) 0.8Cit-HAP

3.2. Adsorption properties

The reactivity of wCit-HAP surfaces determines their surface and interface properties. The adsorption process affects many fields of application, including water treatment, soil treatment and the environment. The surface/interface plays an important role in understanding the mechanisms of interactions and exchanges between adsorbent/solute. To control wCit-HAP surface, MB dye was used as a pollutant model.

The adsorption equilibrium time was determined by putting in contact the MB solutions with Cit-HAP for different times at room temperature (25°C) (**Fig. 6**). The MB adsorption rate is fast in the first 30 min due to the presence active sites available on the grafted materials. After that, the rate of increase decreased and eventually reaches equilibrium at about 60 min because the sites tend to be saturated and the removal rate no longer increased. A good MB removal is observed for 0.2Cit-HAP. The adsorbent surface contains hydroxyl and carboxyl groups can considerably affect the adsorption mechanisms of the dye on the wCit-HAP powders [38]**.**

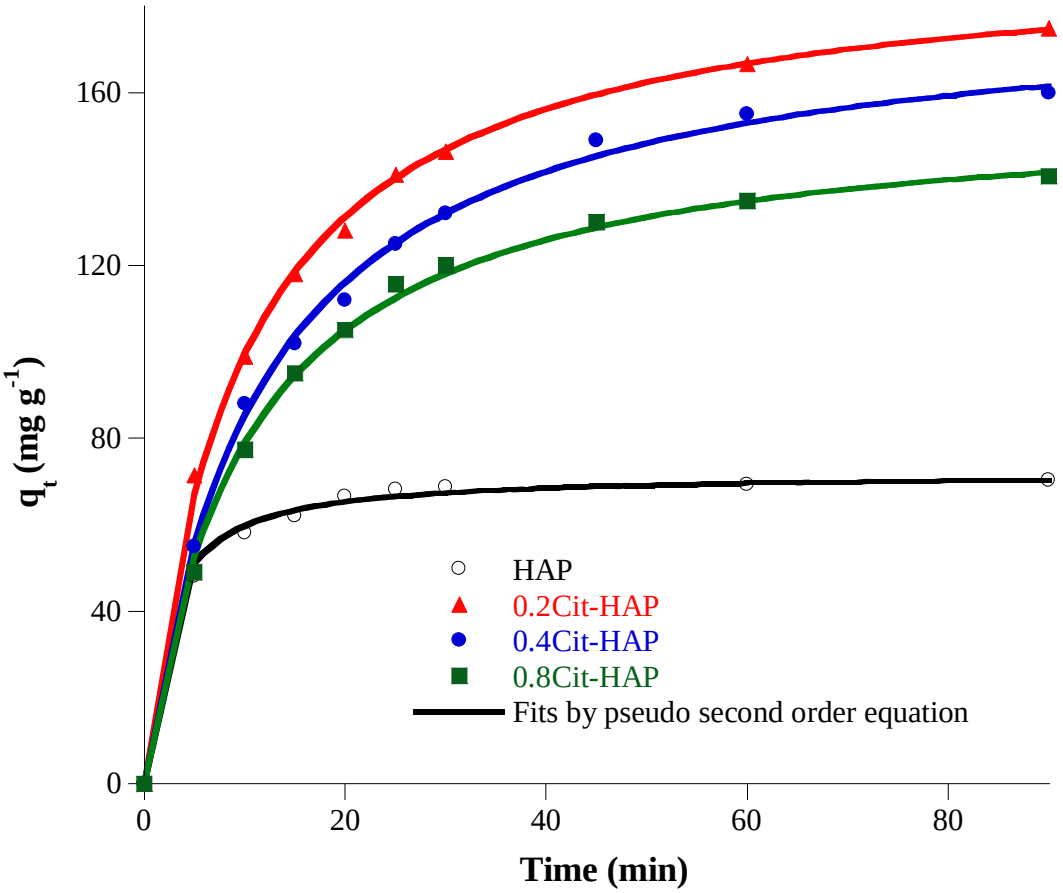

Figure 6. Kinetics of MB removal (q_t) by HAP and wCit-HAP powders, Plain lines are data fitting to the pseudo-second order Lagergren model.

To fit the kinetic data, various models, namely: pseudo-first-order (Eq.2); pseudo-second-order (Eq.3) and Elovich (Eq.4) and expressed respectively as follows: $\log(q_e - q_t) = \log q_{e,1} - \frac{k_1}{2.303}t$: (Eq.2) ; $\frac{t}{q_t} = \frac{1}{k_2.q_e^2} + \frac{t}{q_e}$ (Eq.3) ; $q_t = \frac{1}{\beta}ln(\alpha\beta) + \left(\frac{1}{\beta}\right)ln(t)$ (Eq.4)**,** where q_t (mg g^{-1}) and q_e (mg g^{-1}) are the adsorption capacities at t time (min) and at equilibrium time, respectively. k_1 (min^{-1}) and k_2 (mg g^{-1}·min^{-1}) are the rate constants of adsorption from Eqs.1 and 2, respectively and $q_{e,i}$ (mg g^{-1}) their equilibrium adsorption capacities. α (mg g^{-1} min^{-1}) is the initial adsorption rate and β (g mg^{-1}) the desorption constant. The error functions employed were as follows [39]: (i) Chi-square test $X^2 = \sum_{i=1}^{N}\frac{(q_{e,exp}-q_{e,cal})^2}{q_{e,cal}}$ (Eq.5); (ii) Residual root means square error $RMSE = \sqrt{\frac{1}{N-2}\sum_{i=1}^{N}(q_{e,exp}-q_{e,cal})^2}$ (Eq.6)**;** and (iii) Average percentage error $APE\ (\%) = 100 \times \frac{1}{N}\sum_{i=1}^{N}\left|\frac{q_{e,exp}-q_{e,cal}}{q_{e,exp}}\right|$ (Eq.7)

For each kinetic model to be the most suitable, it will be necessary that the parameters thus provide the smallest sum of normalized error. The experimental values and the linear

adjustment parameters of these models retained with their corresponding error functions are grouped together in **Table 3.**

Table 3. Kinetic parameters for BM dye adsorption on HAP and wCit-HAP

		HAP	0.2Cit-HAP	0.4Cit-HAP	0.8Cit-HAP
$q_{e,exp}$ (mg g^{-1})		70.3	175.0	160.0	140.6
Pseudo first-order	$q_{e,1}$ (mg g^{-1})	13.2	142.5	125.8	107.6
	k_1 (min^{-1})	0.026	0.036	0.028	0.033
	R^2	0.7262	0.9709	0.966	0.9343
	APE (%)	3.31	6.36	1.49	1.58
	χ^2	2.84	7.83	2.77	6.07
	RMSE	4.46	12.6	6.76	8.88
Pseudo second-order	$q_{e,2}$ (mg g^{-1})	71.9	192.3	181.81	151.5
	k_2(g $mg^{-1}min^{-1}$)	0.0068	0.0005	0.0004	0.0006
	R^2	0.9997	0.9998	0.9990	0.9994
	APE (%)	1.69	0.922	0.747	1.29
	χ^2	0.835	0.373	0.513	0.731
	RMSE	2.6	2.25	2.88	2.67
Elovich	$\alpha.10^3$ (mg g^{-1} min^{-1})	1.897	0.058	0.037	2.09
	β (g mg^{-1})	0.135	0.027	0.026	0.107
	R^2	0.8202	0.9834	0.9804	0.8452
	APE (%)	5.56	3.13	1.49	10.10
	χ^2	3.09	1.85	1.54	27.73
	RMSE	5.15	6.27	5.34	19.50

According to the correlation coefficients (R^2), χ^2, RMSEE, and APR values of three models tested, the pseudo- second-order model (k_2 and $q_{e,2}$) proved to be well suited to reproduce MB adsorption kinetic data on w-Cit-HAP. Moreover, the theoretical values $q_{e,th}$ resulting from the pseudo-first order equation are far from the $q_{e,exp}$ whereas the pseudo-second order model has well described the MB adsorption on grafted materials. This indicates that the kinetics of MB adsorption on Cit-HAPs depends on the availability of active sites. Based on the minimum sum of χ^2, RMSE and APE errors from a pseudo-second-order model suggest that

chemical interactions MB////Cit-HAP are dominant [40, 41] despite electrostatic interactions and that hydrogen bonds may contribute to the adsorption mechanism.

The influence of adsorbent weight was studied in the 20-500 mg range (**Fig.7**). Results show that a mass of 50 mg of material is capable of fixing the maximum of MB (90%). The amounts of attached dye must be consistent with the doses of adsorbent in solution to ensure an equivalent number of adsorption sites. With the further increase in the dose of adsorbent, there is an agglomeration of the particles which affects the surface via its active sites which become saturated, hence a low adsorption capacity. It is therefore useful to work with an adsorbent dose of less than 50 mg and to avoid an ineffective overdose. Thus, 50 mg of sorbent mass in 100 mL of MB solution was used corresponding to 0.5 g L^{-1} as sorbent dose.

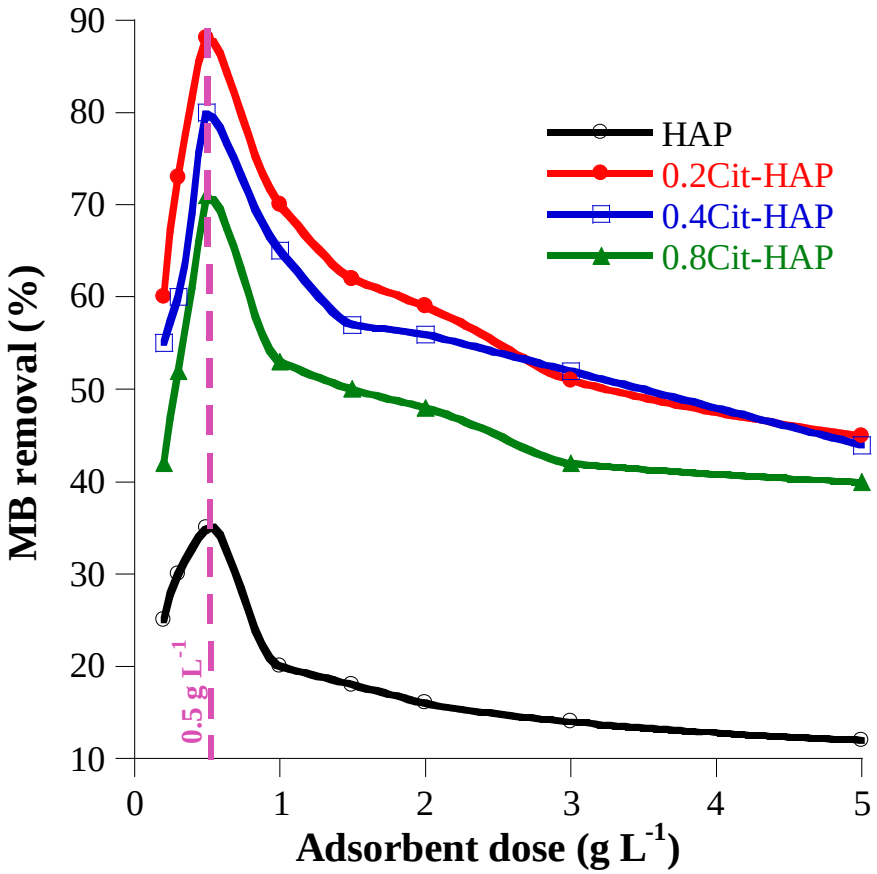

Figure 7. Effect of adsorbent dose on removal of MB dye from aqueous

The initial pH of MB solutions affects the degree of ionization, adsorption mechanism, charge, and activity of surface functional groups. Adsorption of MB onto wCit-HAP powders at different pH are shown in **Figure 8a**. The MB removal reaches its maximum around pH 8, and then a slight drop in efficiency is observed with the increase in pH. To elucidate the nature of the charge carried on the surface of the adsorbent, the determination of the point of

zero charge or pH_{PZC} was carried out. The determination of pH_{PZC} is very important in the phenomena of adsorption, in particular when electrostatic forces intervene in the mechanisms, which is the case of organic pollutants with hybrid apatites. The **Figure 8b** shows that the pH_{PZC} of the grafted apatites varies slightly according to the initial pH but it is between 7.5 and 8.

At strongly acidic pH, the surface of the grafted apatite being protonated and positively charged disadvantages MB-adsorption. This is due to a competitive adsorption between the MB^+ of the MB molecules and the H_3O^+ cations in solution. With pH increasing before pH_{PZC}, it can decrease of repulsion of charge and then the adsorption capacity increases. At $pH>pH_{PZC}$, the surface of the grafted material becomes negatively charged, and the adsorption is then significant related to the increased electrostatic repulsion between the aromatic cations MB^+ from MB molecules and oxygen from hydroxyl OH and carboxylate (COO^-) at Cit-HAP surface. This is in good agreement with the increase in negative surface charge. This explains why the retention is more remarkable when the pH close to 8, but this efficiency, as a function of pH, is quite complex and far from being a simple electrostatic mechanism between oppositely charged species. A fall of Methylene blue adsorption on the wCit-HAP at pH higher than 8 is observed. This is related to the repulsion that occurs between the negatively charged wCit-HAp surface and the MB dye in the solution also acquired a negative charge. Similar results were also observed by various authors [42-44].

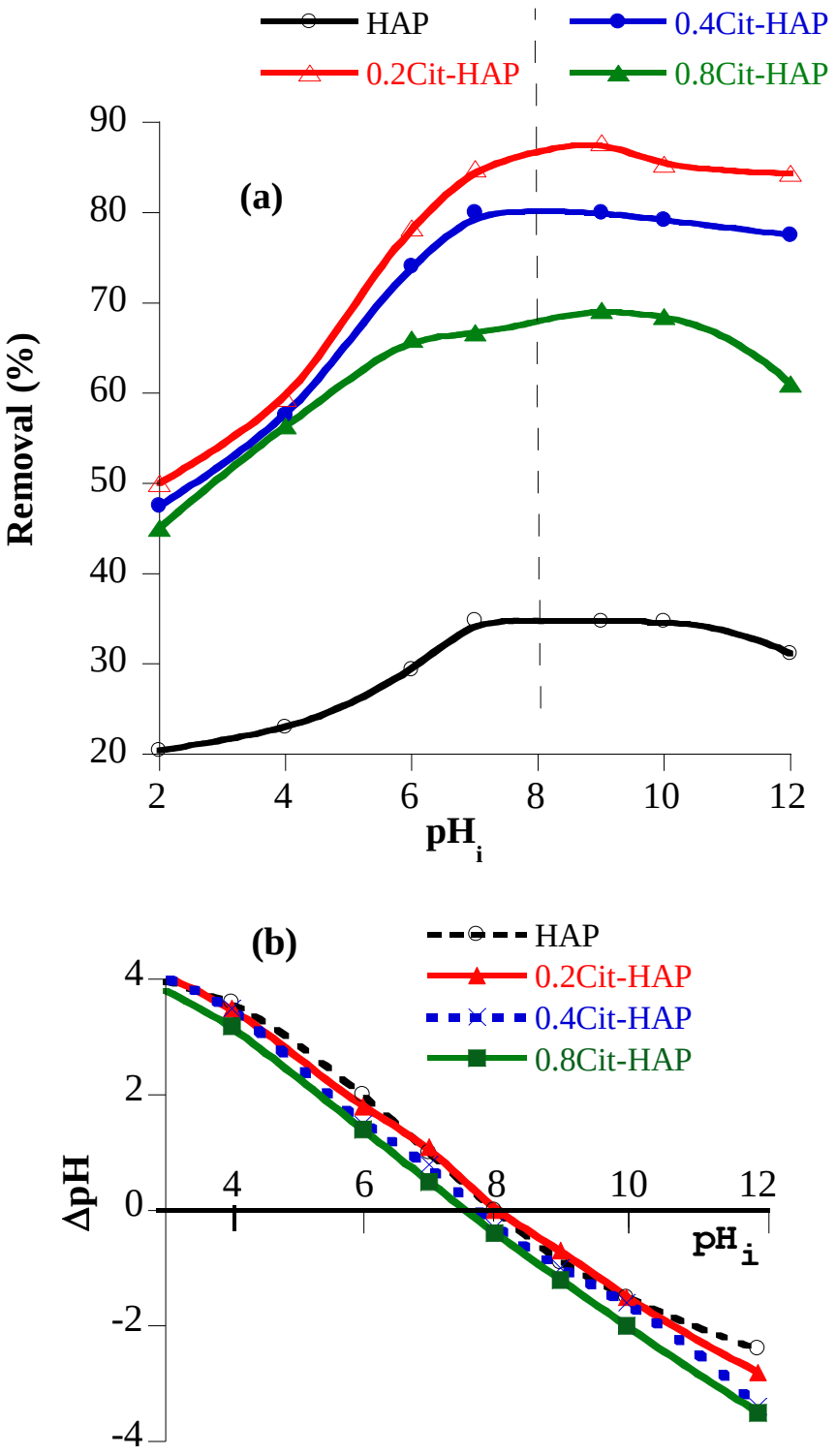

Figure 8. (a) pH effect on MB adsorption, and (b) charge surface of HAP, and wCit-HAP adsorbents. C_0(MB) = 100 mL; adsorbent dose=0.5 g L^{-1}, room temperature (298 K); contact time= 3h.

According to the experimental conditions described above, the **Figure 9** shows the MB adsorption isotherms on Cit-HAP adsorbents**.** The adsorption capacity increases progressively

with the initial MB concentration without saturation level; this indicates that the adsorbents adsorb more if there are more MB molecules. As 0.8Cit-HAP powder has a large specific surface area but has a low adsorption capacity compared to 0.2Cit-HAP being the good adsorbent, it should be noted that the specific surface of the adsorbent is not the only parameter to be considered during the elimination of MB molecules from aqueous solutions. Therefore, the chemical composition of the adsorbent surface is the main parameter determining the MB adsorption process.

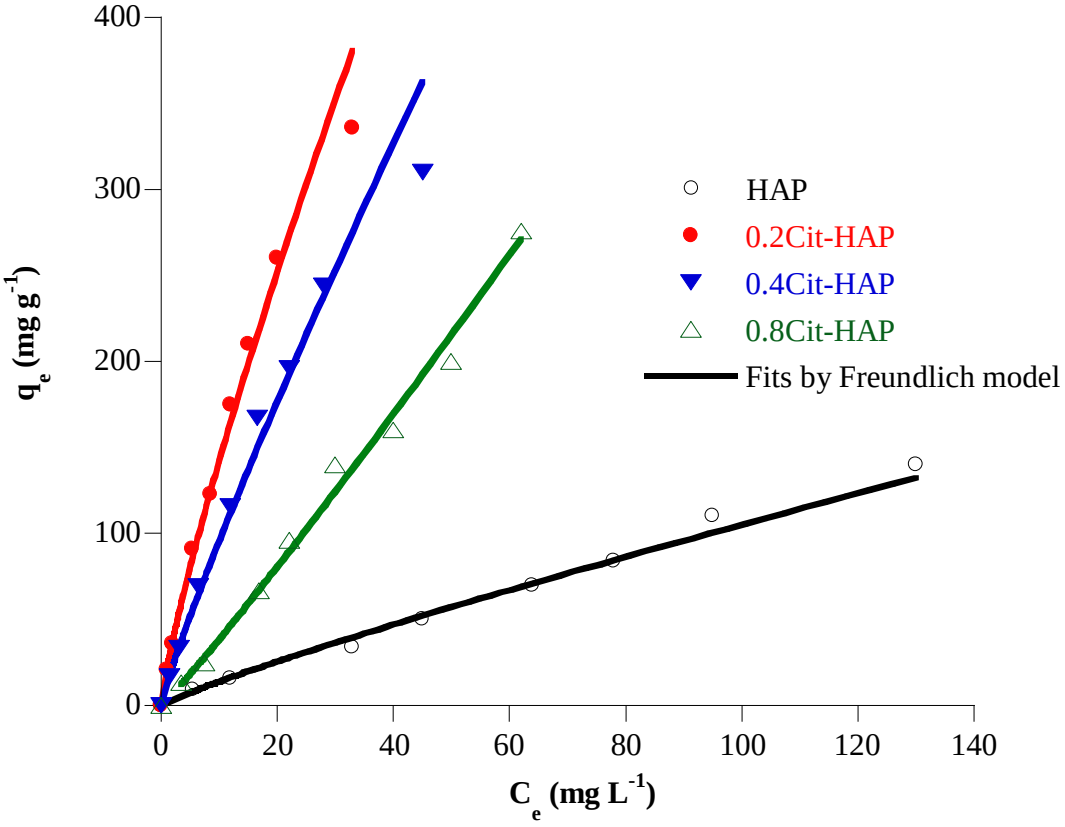

Figure.9. Effect of the initial concentration of MB on their adsorption on HAP and wCit-HAP powders, Plain lines is fitted using the Freundlich-derived equation.

Four models of MB adsorption isotherms on wCit-HAP were discussed [45, 46]: Langmuir (Eq.8), Freundlich (Eq.9), Dubinin-Radushkevich (Eq.10) and Temkin (Eq.11) (**Table 4**). $\frac{C_e}{q_e} = \frac{1}{b.q_L} + \frac{C_e}{q_L}$ (Eq.8); $Ln\, q_e = Ln\, K_F + 1/n\, LnC_e$ (Eq.9); $Ln\, q_e = Ln\, q_{D-R} - \beta(RTLn(1 + \frac{1}{C_e})^2$ (Eq.10); $q_e = \left(\frac{RT}{b_T}\right) ln(A_T C_e)$ (Eq.11), where q_e (mg g^{-1}) the amount of the adsorbate at equilibrium, C_e (mg L^{-1}) equilibrium concentration of the adsorbate on the adsorbent, b (L mg^{-1}) refers to the Langmuir constant and q_L (mg g^{-1}) its maximum adsorbate capacity. K_F is (L mg^{-1}) Freundlich constant and 1/n is an indicator of surface heterogeneity. β is the Dubinin-Radushkevich constant and q_{D-R} the theoretical maximum adsorbate capacity (mg g^{-1}) with

$E = \frac{1}{\sqrt{2\beta}}$ corresponds of adsorption energy. b_T (J/mol) is the Temkin constant related to the variation of adsorption energy, A_T (L/mg) is the equilibrium constant of the Temkin model. R was the gas constant (8.314 J/mol·K), and T was the absolute temperature (K).

The validity of models was determined by calculating the standard deviation (SD, %) using $SD(\%) = 100 \times \sqrt{\frac{1}{N-1}\sum_{i=1}^{N}(\frac{q_{e,exp}-q_{e,th}}{q_{e,exp}})^2}$ (Eq.12), where the $q_{e,exp}$ and $q_{e,th}$ refer to the experimental and the calculated data, and N is the number of data points. A correct fitting of the experimental data with Freundlich equation (R^2>0.99 and less SD (%)) was obtained for MB adsorption (**Table 4**), which describes non-ideal reversible multilayer adsorption with a heterogeneous distribution of the heat of adsorption on the heterogeneous surface.

Table 4. Calculated adsorption isotherm values using regression analysis for BM removal

		HAP	0.2Cit-HAP	0.4Cit-HAP	0.8Cit-HAP
Langmuir	q_L (mg g^{-1})	666	1000	500	n.d
	β	0.0019	0.002	0.002	n.d
	R^2	0.3324	0.9225	0.8224	0.4143
	SD (%)	12.0	12.5	27.2	93.30
Freundlich	K_F	1.836	21.210	12.40	3.24
	1/n	0.879	0.8260	0.8870	1.073
	R^2	0.9929	0.9955	0.9932	0.9944
	SD (%)	6.2	6.45	6.02	6.43
Dubinin-Radushkevich	q_m (mg g^{-1})	66.98	173.5	158.99	669.34
	β (mol^2 kJ^{-2})	13.055	0.846	1.589	4.886
	E (kJ mol^{-1})	0.195	0.768	0.561	0.320
	R^2	0.6576	0.7593	0.7369	0.8128
	SD (%)	56.95	55.95	54.78	50.43
Temkin	A_T (L/mg)	0.1341	0.7431	0.4144	0.2042
	b_T (J/mol)	64.589	27.811	36.335	29.428
	R^2	0.8234	0.896	0.9133	0.8504
	SD (%)	80.80	26.34	26.60	42.11

The affinity distribution of all synthesized materials, based on the Freundlich isotherm being the best fitting model was determined according to the following equation: $N\left(\frac{1}{C_e}\right) = \mathrm{N(K)} = \left|\frac{q_e(\alpha C_e)-q_e(\frac{C_e}{\alpha})}{2\log\alpha} - \frac{\alpha}{(\alpha-1)^2}\frac{\left[q_e(\alpha^2 C_e)-q_e\left(\frac{C_e}{\alpha^2}\right)-q_e(\alpha C_e)+q_e(\frac{C_e}{\alpha})\right]}{2\log\alpha}\right|$ (Eq.13); were q_e (mol g^{-1}) and C_e (mol L^{-1}) is the adsorption quantities and concentration dye in equilibrium respectively and α is equal to$10^{0.2}$.

The plotted curves N(K) vs. Ln(K) and Ln(N(K)) vs. Ln(K) curves give a similar affinity distribution (**Figure 10**). Given the uncertainty of the graphs (N(K) = ±1–5%), the experimental and calculated distributions are indistinguishable. It shows the binding sites energy distribution of the HAP and wCit-HAP determined using Freundlich isotherm obtained from adsorption experiments. This isotherm assumes that the binding affinities of the different types of adsorption sites are exponential distribution. Moreover, it can be observed that both graphs suggest that the BM dye molecules are adsorbed on the binding sites with different binding energies. More specifically, based on N(K) = f(Ln(K)) graphs, the exponential distribution of the binding site energies suggests that the all materials surface is highly heterogeneous and that the adsorbing molecules of BM dye are occupied on the binding sites with high energy. However, the exponential distribution of the binding sites obtained by the equation 13 follows a similar trend for all materials, suggesting that the difference in magnitudes is only due to the difference in the terms preceding the exponent in this equation. This could be confirmed from the parallel lines in an Ln-Ln plot as in Figure 10b. The parallel lines imply that the underlying exponential functions have the same exponents, indicating the heterogeneity of the adsorbents.

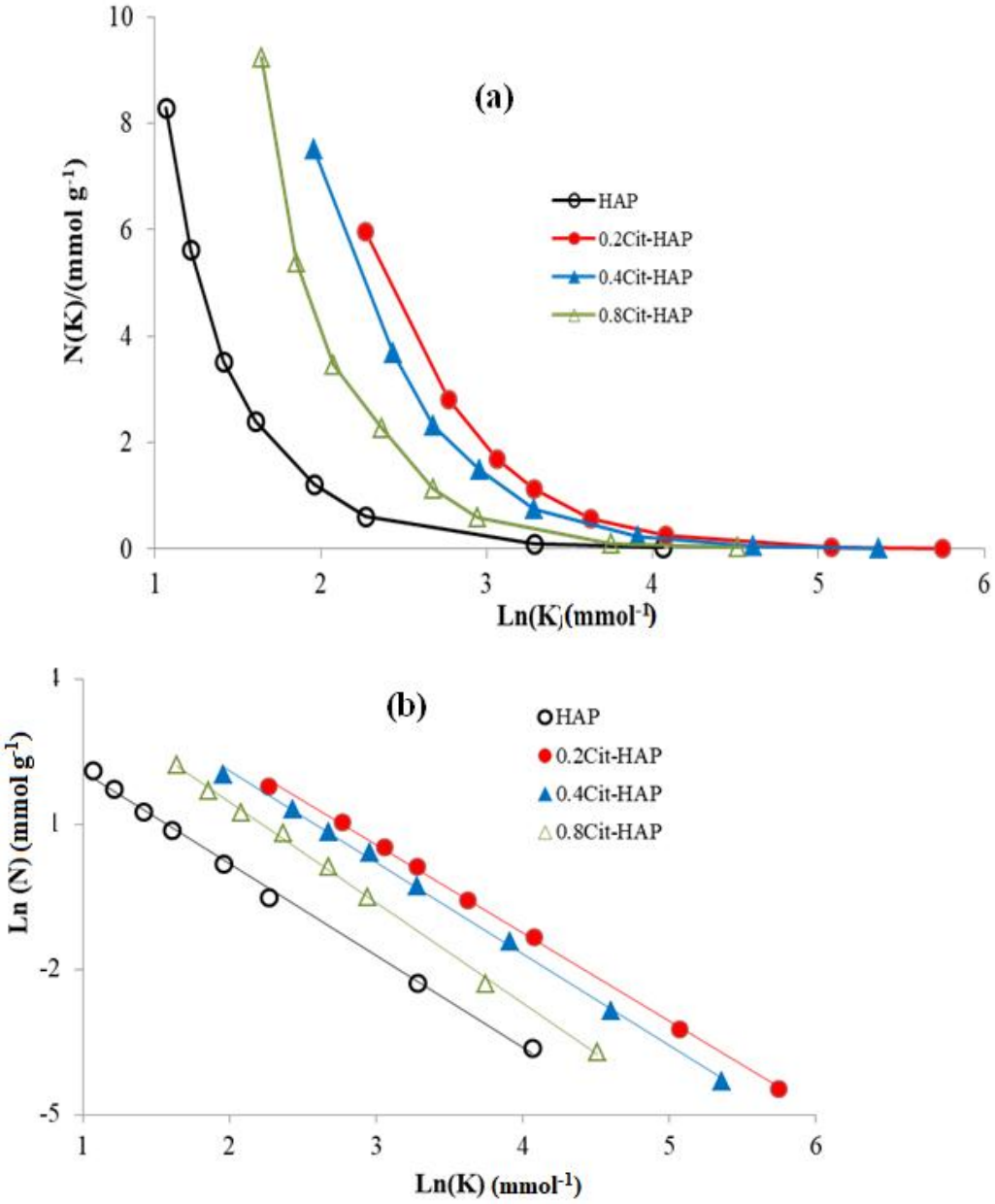

Figure 10. Affinity distribution curves calculated using the AS method for HAP and wCit-HAP plotted in (a) N(K) vs. Ln (K) and (b) Ln(N(K)) vs. Ln (K).

For HAP/MB and wCit-HAP/ MB interactions, the affinity distribution in N(K) vs Ln(K) format was an exponentially decreasing function. For the highest association constant ($K=1/C_{e,min}$) the affinity distribution tends to zero while it tends to infinity for the lowest association constant ($K=1/C_{e,max}$). The Ln(N(K)) versus Ln(K) plots are straight lines, suggesting that the Freundlich model is consistent with the adsorption energy distribution.

By varying the temperature of the MB adsorption reaction on wCit-HAP and by calculating the equilibrium constant $K_d=q_e/C_e$ at each temperature from 25-50°C, the thermodynamic parameters, $\Delta S°$ and $\Delta H°$, were calculated from the slope and intercept of the linear plot of Ln

K_d versus 1/T according to the Van't Hoff equation Ln $K_d = \Delta S^\circ/R - \Delta H^\circ/RT$ (**Figure 11**). At given temperature, the free enthalpy (kJ mol^{-1}) was then calculated as $\Delta G° = \Delta H° - T\Delta S°$ and the calculated thermodynamic parameters were given in **Table 5**.

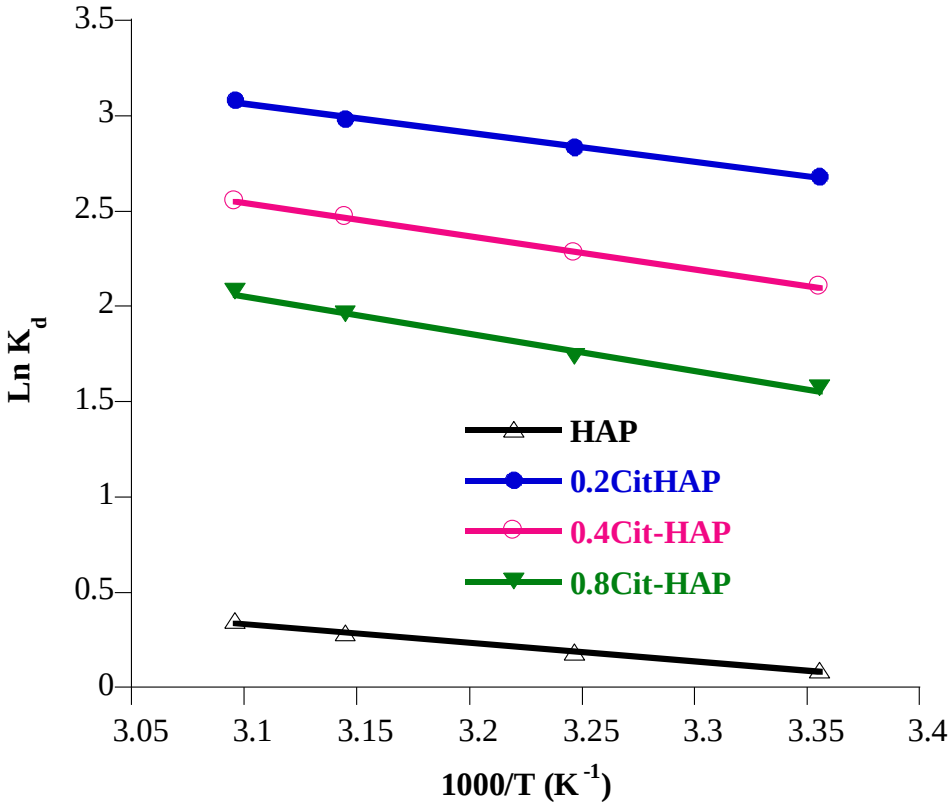

Figure. 11. Effect of temperature on the adsorption of MB on wCit-HAP (Adsorbent dose=0.5 gL^{-1}, initial MB concentration = 100 mg L^{-1}, and pH 7)

As shown in figure 11, the adsorption process is thermally activated. When the temperature of (MB + wCit-HAp) reaction increases, the MB molecules are therefore more agitated, and they move more quickly towards the wCit-HAP surface and the adsorption process takes place more quickly. Endothermic chemical transformations only occur if the system receives thermal energy from the external environment. The temperature of the chemical system decreases. All the enthalpies ΔH° and ΔS° obtained are positive, indicating that the MB adsorption on HAP and wCit-HAP is an endothermic process. These energies increase with the grafted citrate content. The positive values of $\Delta S°$ revealed a creation of a random disorder via an increase in the degrees of freedom of the molecules at "Solution/wCit-HAP" interface during the transfer of MB^+ ions towards the active sites of the adsorbent surface. The negative values of ΔG calculated at selected temperatures show that the dye adsorption process on all materials is a favorable and spontaneous process and are between -8.277 and -26.70 kJ mol^{-1}. All the $\Delta H°$ values are lower than 20 kJ mol^{-1}, indicating that there are weak

electrostatic Van der Waals forces as well as the formation of hydrogen bonds, whose mechanism is of the physisorption type. This thermodynamic approach clearly indicates that the MB desorption from the Cit-HAP surface is easily achievable, requiring only a simple chemical treatment.

Table 5. Thermodynamic parameters

	HAP	0.2Cit-HAP	0.4Cit-HAP	0.8Cit-HAP
$\Delta H°$ (kJ mol^{-1})	8.28	12.64	14.38	16.20
$\Delta S°$ (J mol^{-1} K^{-1})	28.48	64.66	65.70	67.30
$\Delta G°_{298}$ (kJ mol^{-1})	-8.47	-19.25	-20.87	-21.72

3.3. Reuse of adsorbents

Reusing materials is an important feature that should be considered in adsorption process. Many chemical agents have been applied to regenerate adsorbents such as acids, alkalis, salts and organic solvents. The reusability of wCit-HAP adsorbents was verified by adsorption-desorption tests over four cycles for MB. The adsorption efficiency in each cycle was analyzed (**Figure 12**). The 0.2Cit-HAP retained good adsorption capacity after repeated cycles of adsorption-regeneration with little difference, which does not exceed 1-2%. This indicates that there are almost reversible sites onto adsorbent surfaces. Recyclability studies suggest that wCit-HAP can be used repeatedly as effective adsorbents in wastewater treatment.

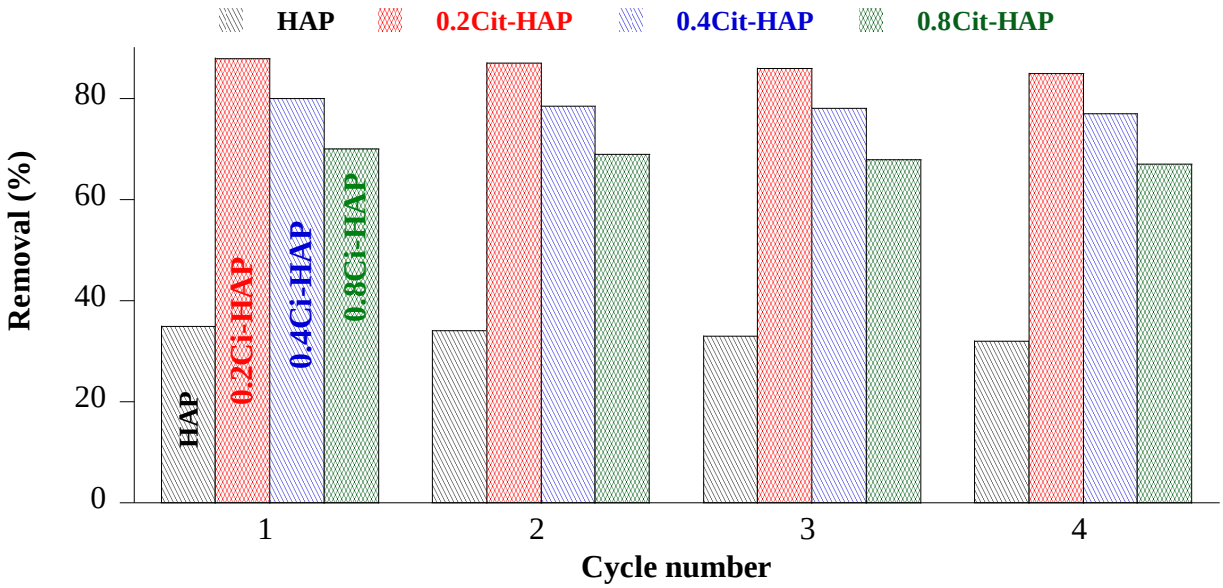

Figure 12. Regeneration of materials on the yield of adsorption of the dye.

After adsorption, the adsorbents (HAP and wCit-HAP) were washed several times with distilled water and then with 3.0 M NaOH. The regenerated materials were washed with distilled water, dried at 80°C and subsequently tested in MB adsorption. As shown in **Figure 12**, the removal yield of the wCit-HAP does not significantly change during the adsorption–desorption recycling (<5%). This shows that reuse of the wCit-HAP material is a simple operation and can be used multiple times.

3.4. DFT study

The quantum chemical calculations performed by DFT were carried to investigate the relationship between the electronic structure and the adsorption process of MB (**Figure. 13)** onto the HAP and wCit-HAP materials.

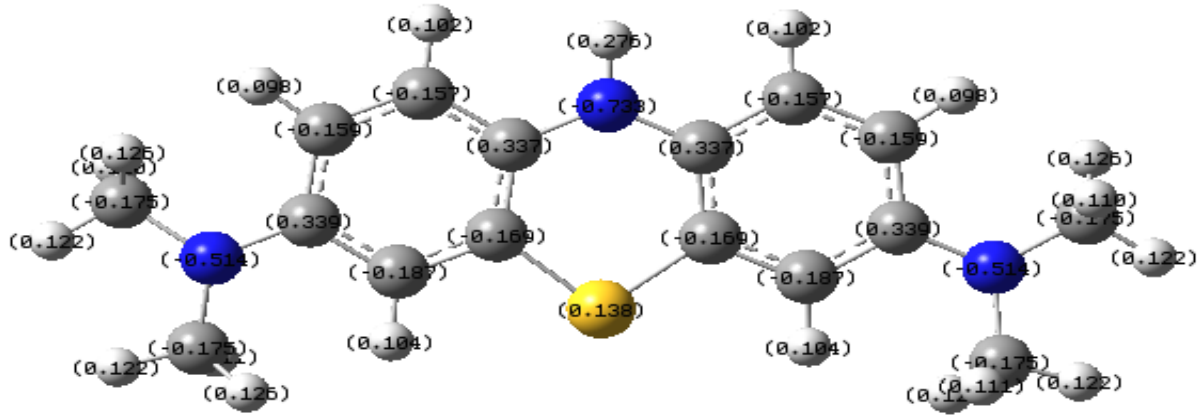

Figure 13. Mulliken atomic charges distribution (e^-) of optimized molecular geometries of methylene blue.

To determine the electrophilic properties and the nucleophilic sites as well as the hydrogen bonding interactions of the materials studied, an electrostatic potential (ESP) map is important. Different colors indicate negative and positive sites ranging from red to dark blue. The color code of the ESP diagrams lies between –7.509e^2 a.u. (Dark red) and 7.509e^2 a.u. (Dark blue) for MB, HAP and 0.2Cit-HAP. The dark blue region around nitrogen atoms of protonated MB molecule represents their negatively charged (nucleophilic). These electron-rich areas would be the preferred sites for adsorption to the HAP and Cit-HAP surface.

Figure 14 presents the optimized structures, HOMO, LUMO densities and ESP maps of the studied molecular systems: the red and blue colors indicate the negative and positive phases of the studied structures respectively. Through computation of electronic charge distribution, the interactions between phosphate groups (PO_4^{3-}) and BM dye are considered as background knowledge due to acid–basic interaction due to hydrogen bonding as well as adsorption by

dispersion forces as a principal of electrostatic interactions and ion**.** In **Table 6**, we presented all quantum chemical indices of the studied materials.

Table 6. Quantum chemical descriptors for MB, HAP and Cit-HAP

	E_{HOMO} (eV)	E_{LUMO} (eV)	ΔE_{gap} (eV)	η (eV)	μ (eV)	χ	ω (eV)	ΔN_{max}
MB	-4.162	-0.267	3.894	11.57	-2.214	2.214	2.136	1.930
HAP	-4.319	-1.172	3.147	4.947	-2.746	2.746	2.395	1.744
Cit-HAP	-4.670	-1.989	2.680	1.340	-3.329	3.329	4.135	2.484

According to the obtained ΔE_{gap} values, it can be observed that HAP and Cit-HAP are reactive in the aqueous phase but Cit-HAP (ΔE_{gap} = 2.68) is more reactive. The maximum charge transfer of Cit-HAP (ΔN_{max}=2.484) is greater than that of HAP (ΔN_{max}=1.744). The electrophilic gap difference between the two reagents MB-HAP (Δw =0.258) is very small. On the other hand, the difference of global electrophile between MB-Cit-HAP is very important (Δw =1.998) which indicates an important polar character in this adsorption dye [47]. Compared by HAP, the lowest hardness value was obtained for Cit-HAP (η=1.340) which shows the greater reactivity of these molecules compared by those of HAP. The obtained values of η and χ emphasize that the dye has a remarkable chemical reactivity and adsorption affinity for the Cit-HAP surface indicating a higher electrophilicity value [48, 49].
In order to further understand its high MB adsorption capacity on hybrid materials, electrostatic potential (ESP) proprieties of the MB and wCit-HAP was conducted by the DFT calculation. Electrostatic attraction with a negatively charged adsorbent surface like phosphate (PO_4^{3-}) is well shown: the MB molecules will have a tendency to orient itself preferentially to the surface by the sides possessing the highest values of positive charge density**.** The strong H-bonding interaction between the P-OH groups of wCit-HAP and the nitrogen atom of the MB molecules was contributed to the adsorption of the dye molecules. The nitrogen atoms of MB were interacting with Ca^{2+} of wCit-HAP via Lewis acid-base interaction. The quantum chemical calculations were employed to explore the intermolecular interactions involved in the adsorption MB on HAP and wCit-HAP surface. The frontier molecular orbitals were investigated to analyze the HOMO and LUMO (**Figure 14**). It was visualized that both HOMO and LUMO orbitals were widely distributed on the area of the MB molecules and on the oxygen atoms of the HAP and wCit-HAP, which indicates that these sites present the active sites of adsorption. This result was confirmed by the molecular electrostatic potential maps (MEP). Furthermore, the molecules with small gap energetic explain the reactivity

performance of these molecules [32]. In our case, it can be noticed that Cit-HAP a small gap energetic compared to HAP which leads us to suggest that the Cit-HAP had a high reactivity to remove better the dye.

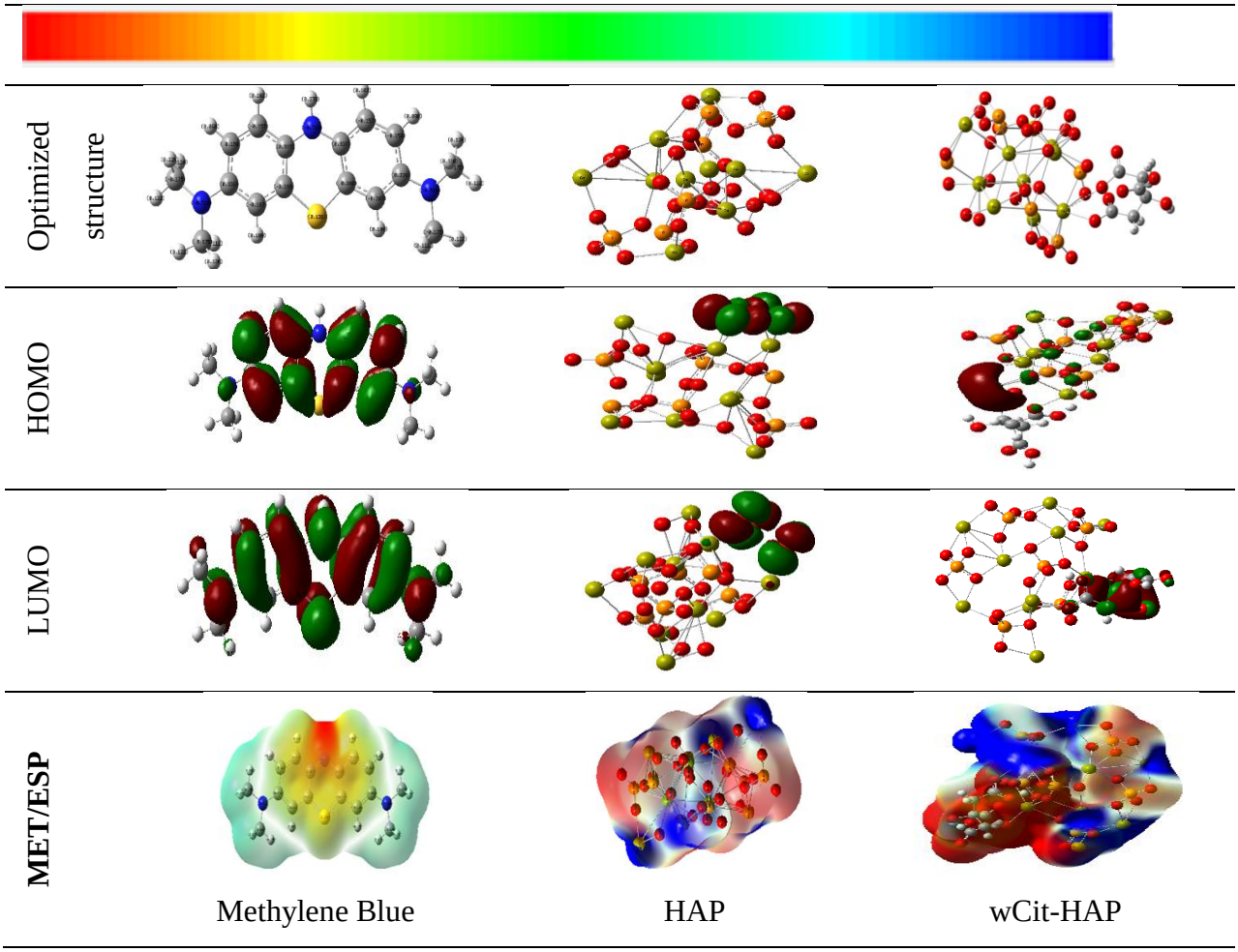

Figure14. The optimized structure, HOMO, LUMO and MEP/ESP for methylene blue, hydroxyapatite and wCit-HAP.

3.5. Comparison of adsorption capacity

A comparative study between the materials synthesized in this work and other hydroxyapatite-based and activated carbon materials studied to remove MB was performed. The results have been summarized in Table 7. It was observed from Table 7 that the new hybrid materials synthesized (wCit-HAp) have a higher monolayer adsorption capacity (q_{max}, mg g^{-1}) for the removal of MB dye.

Table 7. Comparison of maximum adsorption capacities for MB dyes by other adsorbents.

Adsorbent	Adsorption capacity q_{max} (mg g^{-1})	Ref.
Silver nanoparticles loaded on activated carbon	75.2	[50]
Activated carbon from mangosteen peels (MSPAC)	163.6	[51]
Banana stem based activated carbon	101.01	[52]
Activated carbon from oak seeds	24	[53]
Hydroxyapatite	50.25	[54]
Activated carbon from stem palm fibres	110.79	[55]
Poorly crystalline HAP	14.27	[56]
Microwave-HAP	33.3	[57]
Nano Hydroxyapatite/Chitosan Composite	30.2	[58]
Magnetic chitosan	60.4	[59]
Alginate–Chitosan–Montmorillonite	137.15	[60]
Activated carbon from sugarcane bagasse waste	136.5	[61]
HAP	70	This work
0.2Cit-HAP	173	This work
0.4Cit-HAP	167	This work
0.8Cit-HAP	140	This work

4. Conclusion

This work provides fundamental data on synthesized hybrid hydroxyapatites and their adsorption efficiency. The charged state of the hydroxyapatite surface plays an important role in MB trapping. The grafting of citrate from citric acid makes it possible to anchor to the HAP surface with the three carboxylate functions, and better promotes the retention of neighboring species in solution. The results obtained indicate that the in-situ grafting of citrate groups within HAP matrix is an interesting way for water pollution control. They revealed some important features:

(i) the amount of citrate fixed on the HAP surface strongly influences the structural and adsorption properties,

(ii) (ii) The adsorption kinetics for the hybrid materials show that the pseudo-second order provides the best fit to the experimental data, while the Freundlich model fits the experimental data of the adsorption isotherms,

(iii) (iii) Based on the thermodynamic data, a physisorption mechanism was discussed through the weak Van de Waals-like electrostatic forces and the formation of hydrogen bonds between MB and Cit-HAP hybrid materials, indicating that the MB desorption is easily achievable, requiring only a simple chemical treatment,

(iv) DFT calculations displayed a clear view of the adsorption sites of the wCit-HAP indicating the dye adsorption reaction mechanism could be controlled by charge transfer.

Acknowledgements

This work was financially supported by the European Union (ERDF) and "Région Nouvelle Aquitaine". Thanks are due to the University of Monastir (Tunisia) for their continuous support during the realization of this work.

References

[1] S. Sun, T. Jiang, Y. Lin, J. Song, Y. Zheng, D. An, Characteristics of organic pollutants in source water and purification evaluations in drinking water treatment plants, Sci. Total Environ. 733 (2020) 139277. https://doi.org/10.1016/j.scitotenv.2020.139277.

[2] P. Luo, B. Zhang, Y. Zhao, J. Wang, H. Zhang, J. Liu, Removal of methylene blue from aqueous solutions by adsorption onto chemically activated halloysite nanotubes, Korean J. Chem. Eng. 28 (2011) 800-807. https://doi.org/10.1007/s11814-010-0426-x.

[3] I. Es-saidi, A. Oulguidoum, C. El Bekkali, H. Bouyarmane, A. Laghzizil, J-M. Nunzi, Characterization and valorization of natural phosphate in removing of heavy metals and toxic organic species from water, J. African Earth Sci. 173 (2021) 104022, https://doi.org/10.1016/j.jafrearsci.2020.104022.

[4] L. Liang, W.Tan, Y. Xue, F. Xi, X. Meng, B. Hu, J. Du, Effects of magnetic field on selenite removal by sulfidated zero valent iron under aerobic conditions, Sci. Total Environ. 831 (2022) 154755, https://doi.org/10.1016/j.scitotenv.2022.154755.

[5] F. Liu, Y. Lou, F. Xia, B. Hu, Immobilizing nZVI particles on MBenes to enhance the removal of U(VI) and Cr(VI) by adsorption-reduction synergistic effect, Chem. Eng. J. 454 (2023) 140318, https://doi.org/10.1016/j.cej.2022.140318.

[6] F. Liu, S. Wang, B. Hu, Electrostatic self-assembly of nanoscale FeS onto MXenes with enhanced reductive immobilization capability for U(VI) and Cr(VI), Chemical Engineering Journal 456 (2023) 141100, https://doi.org/10.1016/j.cej.2022.141100.

[7] Q. Li, Z. Chen, H. Wang, H. Yang, T. Wen, S. Wang, B. Hu, X. Wang, Removal of organic compounds by nanoscale zero-valent iron and its composites, Science of The Total Environment 792 (2021) 148546, https://doi.org/10.1016/j.scitotenv.2021.148546.

[8] V.K. Gupta, S. Agarwal, T.A. Saleh, Chromium removal by combining the magnetic properties of iron oxide with adsorption properties of carbon nanotubes, Water Res. 45 (2011) 2207-2212. https://doi.org/10.1016/j.watres.2011.01.012

[9] M. Mansoorianfar, H. Nabipour, F. Pahlevani, Y. Zhao, Z. Hussain, A. Hojjati-Najafabadi, H. Y. Hoang, R. Pei, Recent progress on adsorption of cadmium ions from water systems using metal-organic frameworks (MOFs) as an efficient class of porous materials, Environ. Res. 214 (2022) 114113. https://doi.org/10.1016/j.envres.2022.114113.

[10] A. Mehri, S.B. Moussa, A. Laghzizil, J.M. Nunzi, B. Badraoui, A new in situ enhancement of the hydroxyapatite surface by Tyramine: Preparation and interfacial properties. Colloids Surf. A 592 (2020) 124590. https://doi.org/10.1016/j.colsurfa.2020.124590.

[11] W. Wei, X. Zhang, J. Cui, Z. Wei, Interaction between low molecular weight organic acids and hydroxyapatite with different degrees of crystallinity, Colloids Surf. A 392 (2011) 67-75. doi:10.1016/j.colsurfa.2011.09.034.

[12] A. Oulguidoum, K. Bouiahya, H. Bouyarmane, A. Talbaoui, J-M. Nunzi, A. Laghzizil,Mesoporous nanocrystalline sulfonated hydroxyapatites enhance heavy metal removal and antimicrobial activity, Sep. Purif. Technol. 255 (2021) 117777. https://doi.org/10.1016/j.seppur.2020.117777.

[13] A. Ragab, I. Ahmed, D. Bader, The removal of brilliant green dye from aqueous solution using nano Hydroxyapatite/Chitosan composite as a sorbent, Molecules 24 (2019) 847. https://doi.org/10.3390/molecules24050847.

[14] K. Bouiahya, A. Oulguidoum, A. Laghzizil, M. Shalabi, J.M. Nunzi, Sylvie MASSE, Hydrophobic chemical surface functionalization of hydroxyapatite nanoparticles for naphthalene removal, Colloids Surf. A 595 (2020) 124706, https://doi.org/10.1016/j.colsurfa.2020.124706.

[15] N. Salehpour, M.R. Bayatloo, S. Nojavan, Magnetic solid-phase extraction of high molecular weight peptides using stearic acid–functionalized magnetic hydroxyapatite nanocomposite: determination of some hypothalamic agents in biological samples. Anal. Bioanal. Chem. 413 (2021) 7609-7623. https://doi.org/10.1007/s00216-021-03725-6.

[16] Z. Zhao, X. Zhang, D. Ruan, H. Xu, F. Wang, W. Lei, M. Xia, Efficient removal of heavy metal ions by diethylenetriaminepenta (methylene phosphonic) acid-doped

hydroxyapatite, Sci. Total Environ. 849 (2022) 157557. https://doi.org/10.1016/j.scitotenv.2022.157557.

[17] S. Saoiabi, A. Gouza, H. Bouyarmane, A. Laghzizil, A. Saoiabi, Organophosphonate-modified hydroxyapatites for Zn(II) and Pb(II) adsorption in relation of their structure and surface properties, J. Environ. Chem. Eng. 4 (2016) 428-433, https://doi.org/10.1016/j.jece.2015.11.036.

[18] H. Tanaka, M. Futaoka, R. Hino, Surface modification of calcium hydroxyapatite with pyrophosphoric acid, J. Colloid. Interface Sci. 69 (2004) 358. https://doi.org/10.1016/j.jcis.2003.07.039.

[19] H. Tanaka, A. Yasukawa, K. Kandori, T. Ishikawa, Surface modification of calcium hydroxyapatite with hexyl and decyl phosphates, Colloids Surf. A 125 (1997) 53-62. https://doi.org/10.1016/S0927-7757(96)03876-9.

[20] H.W. Choi, H. J. Lee, K.J. Kim, H.M Kim, S.C Lee, Surface modification of hydroxyapatite nanocrystals by grafting polymers containing phosphonic acid groups, J. Colloid. Interface Sci. 304 (2006) 277. doi: 10.1016/j.jcis.2006.05.069.

[21] L. El Hammari, A. Laghzizil, P. Barboux, A. Saoiabi , M. Meyer, Chemical modification of porous calcium hydroxyapatite surfaces by grafting phenylphosphonic and phenylphosphite acids; Colloids Surf. A 289 (2006) 84-88. https://doi.org/10.1016/j.colsurfa.2006.04.009.

[22] L. El Hammari, H. Marroun, A. Laghzizil, A. Saoiabi, C. Roux, J. Livage, T. Coradin Organically modified porous hydroxyapatites: A comparison between alkylphosphonate grafting and citrate chelation, J. Solid State Chem. 181 (2008) 848-854. https://doi.org/10.1016/j.jssc.2008.01.030.

[23] W. Wei, R. Sun, Z. Jin, J. Cui, Z. Wei, Hydroxyapatite-gelatin nanocomposite as a novel adsorbent for nitrobenzene removal from aqueous solution, Appl. Surf. Sci. 292 (2014) 1020-1029. https://doi.org/10.1016/j.apsusc.2013.12.127.

[24] G. Vasugi, E.K. Girija, Investigations on textile dye adsorption onto hydroxyapatite-alginate nanocomposite prepared by a modified method, Cellulose Chem. Technol. 49 (2015) 87-91.

[25] K. Sangeetha, G. Vasugi, E.K. Girija, Removal of lead ions from aqueous solution by novel hydroxyapatite/alginate/gelatin composites, Int. J. Chem. Tech. Res. 8 (2015) 117–125.

[26] S. Saoiabi, S. El Asri, A. Laghzizil, T. Coradin, K. Lahlil, Nanoporous surface of organofunctionalized hydroxyapatite fabricated from natural phosphate rock , Materials Letters 64 (2010) 2679-2681. https://doi.org/10.1016/j.matlet.2010.09.013

[27] S.B. Moussa, H. Bachouâ, M. Gruselle, P. Beaunier, A. Flambard, B. Badraoui, Hybrid organic-inorganic materials based on hydroxyapatite structure, J. Solid State Chem. 248 (2017) 171-177. https://doi.org/10.1016/j.jssc.2017.02.004.

[28] J. Prywer, M.Olszynski, E. Mielniczek-Brzóska, Inhibition of precipitation of carbonate apatite by trisodium citrate analysed in base of the formation of chemical complexes in growth solution, J. Solid State Chem. 231 (2015) 80-86, https://doi.org/10.1016/j.jssc.2015.08.010.

[29] P. Yu, F. Lu, W. Zhu, D. Wang, X. Zhu, G. Tan, X. Wang, Y. Zhang, L. Li, C. Ning, Bio-inspired citrate functionalized apatite coating on rapid prototyped titanium scaffold, Appl. Surf. Sci. 313 (2014) 947-953. https://doi.org/10.1016/j.apsusc.2014.06.113.

[30] M. Joudi, H. Nasserlah, H. Hafdi, J. Mouldar, H. Badreddine, M. Mhammedi, M. Bakasse, Synthesis of an efficient hydroxyapatite–chitosan–montmorillonite thin film for the adsorption of anionic and cationic dyes: adsorption isotherm, kinetic and thermodynamic study. SN Appl. Sci. **2** (2020) 1078. https://doi.org/10.1007/s42452-020-2848-3.

[31] L. Herrag, B. Hammouti, S. Elkadiri, A. Aouniti, C. Jama, H. Vezin, F. Bentiss, Adsorption properties and inhibition of mild steel corrosion in hydrochloric solution by some newly synthesized diamine derivatives: Experimental and theoretical investigations, Corros. Sci. 52 (2010) 3042-3051. doi.org/10.1016/j.corsci.2010.05.024.

[32] M. Khnifira, W. Boumya, M. Abdennouri, M Sadiq, M. Achak, G. Serdaroğlu, S. Kaya, S. Şimşek, N. Barka, A combined molecular dynamic simulation, DFT calculations, and experimental study of the eriochrome black T dye adsorption onto chitosan in aqueous solutions, Int. J. Biol. Macromol. 166 (2021) 707-721. https://doi.org/10.1016/j.ijbiomac.2020.10.228.

[33] C. Lee, W. Yang, RG. Parr, Development of the Colle-Salvetti correlation-energy formula into a functional of the electron density. Physical review B, 37 (1988) 785. https://doi.org/10.1103/PhysRevB.37.785.

[34] R.D. Dennington, T.A. Keith, J.M. Millam, "GaussView 5.0, Gaussian" Inc., Wallingford 20 (2008).

[35] A. Bigi, E Boanini, C Capuccini, M Gazzano, Strontium-substituted hydroxyapatite nanocrystals, Inorg. Chim. 360 (2007) 1009-1016. https://doi.org/10.1016/j.ica.2006.07.074.

[36] M.R.T. Filgueiras, D. Mkhonto, N. H. de Leeuw, Computer simulations of the adsorption of citric acid at hydroxyapatite surfaces, J. Cryst. Growth 294 (2006) 60-68. doi:10.1016/j.jcrysgro.2006.05.077.

[37] S. Ben Moussa, A. Mehri, M. Gruselle, P. Beaunier, G. Costentin, B. Badraoui, Combined effect of magnesium and amino glutamic acid on the structure of hydroxyapatite prepared by hydrothermal method. Mater. Chem. Phys. 212 (2018) 21-29. doi:10.1016/j.matchemphys.2018.03.017.

[38] RS. Shertate, P. Thorat, Biotransformation of textile dyes: a bioremedial aspect of marine environment, Am. J. Environ. Sci. 10 (2014) 489-499. doi :10.3844/ajessp.2014.489.499

[39] K.Y. Foo, B.H. Hameed, Insights into the modeling of adsorption isotherm systems, Chem. Eng. J. 156 (2010) 2-10. https://doi.org/10.1016/j.cej.2009.09.013.

[40] Y.S Ho, G McKay, Pseudo-second order model for sorption processes, Process Biochem. 34 (1999) 451-465, https://doi.org/10.1016/S0032-9592(98)00112-5.

[41] Y-H. Li, C-C.Wang, X. Zeng, X.Z Sun, C. Zhao, H. Fu, P. Wang, Seignette salt induced defects in Zr-MOFs for boosted Pb(II) adsorption: universal strategy and mechanism insight, Chem. Eng. J. 442 (2022) 136276, https://doi.org/10.1016/j.cej.2022.136276.

[42] K. Sharma, S. Sharma, V. Sharma, P. K. Mishra, A. Ekielski, V. Sharma, and V. Kumar. Methylene Blue Dye Adsorption from Wastewater Using Hydroxyapatite/Gold Nanocomposite: Kinetic and Thermodynamics Studies, Nanomaterials 11(2021) 1403. https://doi.org/10.3390/nano1106140.

[43] V. Tharaneedhar, P.S. Kumar, A. Saravanan, C Ravikumar, V. Jaikumar. Predict ion and interpretation of adsorption parameters for the sequestration of methylene blue dye from aqueous solution using microwave assisted corncob activated carbon. Sustain. Mater. Technol. 11 (2017) 1-11. https://doi.org/10.1016/j.susmat.2016.11.001.

[44] V.C. Nguyen, Q.H. Po, Preparation of chitosan coated magnetic hydroxyapatite nanoparticles and application for adsorption of reactive Blue 19 and Ni^{2+} ions. Sci. World J. 2014 (2014) 273082. https://doi.org/10.1155/2014/273082.

[45] H. Xu, S. Zhu, K. Lu, H.Jia, M. Xia, F.Wang, Preparation of hierarchically floral ZIF-8 derived carbon@polyaniline@Ni/Al layered double hydroxides composite with outstanding removal phenomenon for saccharin, Chem. Eng. J. 450 (2022) 138127. https://doi.org/10.1016/j.cej.2022.138127.

[46] H. Xu, S. Zhu, M. Xia, F. Wang, X. Ju, Three-dimension hierarchical composite via in-situ growth of Zn/Al layered double hydroxide plates onto polyaniline-wrapped carbon sphere for efficient naproxen removal, J. Hazard. Mater. 423 (2022) 127192, https://doi.org/10.1016/j.jhazmat.2021.127192.

[47] Z. Lakbaibi, H. El Makarim, M. Tabyaoui, A. El Hajbi, Theoretical study of the formation of α-chloroglycidic esters in aliphatic series using the quantum DFT method with B3LYP/6-311G (d, p), Int. J. Res. Sci. Innov. Appl. Sci. 7 (2014) 602-616.

[48] H. Han, W. Wei, Z Jiang, J. Lu, J. Zhu, J. Xie, Removal of cationic dyes from aqueous solution by adsorption onto hydrophobic/hydrophilic silica aerogel. Colloids Surf. A 509 (2016) 539-549. https://doi.org/10.1016/j.colsurfa.2016.09.056

[49] R. Salim, A. Nahlé, F. El-Hajjaji, E. Ech-chihbi, F. Benhiba, F. El Kalai, N.Benchat, H. Oudda, A. Guenbour, M. Taleb, I. Warad, A. Zarrouk, Experimental, density functional theory, and dynamic molecular studies of imidazopyridine derivatives as corrosion inhibitors for mild steel in hydrochloric acid, Surf. Eng. Appl. Electrochem. 57 (2021) 233-254, https://doi.org/10.3103/S1068375521020083.

[50] M. Ghaedi, M. Roosta, AM. Ghaedi, A. Ostovan, I. Tyagi, S. Agarwal, VK. Gupta, Removal of methylene blue by silver nanoparticles loaded on activated carbon by an ultrasound-assisted device: optimization by experimental design methodology. Res. Chem. Intermed. 44 (2018) 2929-2950. https://doi:10.1007/s11164-015-2285-x

[51] A.H. Jawad, SEM. Saber, A.S. Abdulhameed, A. Reghioua, Z.A. ALOthman, L.D. Wilson, Mesoporous activated carbon from mangosteen (Garcinia mangostana) peels by H_3PO_4 assisted microwave: Optimization, characterization, and adsorption mechanism for methylene blue dye removal. Diam. Relat. Mater. 129 (2022) 109389. https://doi.org/10.1016/j.diamond.2022.109389

[52] E. Misran, O. Bani, E.M. Situmeang, A.S. Purba, Banana stem based activated carbon as a low-cost adsorbent for methylene blue removal: Isotherm, kinetics, and reusability. Alex. Eng. J. 61 (2022) 1946-1955. https://doi.org/10.1016/j.aej.2021.07.022

[53] S.A. Borghei, MH. Zare, K. Ahmadi, M.H. Sadeghi, A. Marjani, S. Shirazian, M. Ghadiri. Synthesis of multi-application activated carbon from oak seeds by KOH activation for methylene blue adsorption and electrochemical supercapacitor electrode. Arab. J. Chem. 14 (2021) 102958. https://doi.org/10.1016/j.arabjc.2020.102958

[54] N. Barka, S.Qourzal, A. Assabbane, A. Nounah, Y. Ait-Ichou, Removal of reactive yellow 84 from aqueous solutions by adsorption onto hydroxyapatite, J. Saudi Chem. Soc., 15 (2011) 263-267. https://doi.org/10.1016/j.jscs.2010.10.002.

[55] L.S. Maia, A.L. da Silva, E.S. Carneiro, F.M. Monticelli, F.R. Pinhati, D.R. Mulinari, Activated carbon from palm fibres used as an adsorbent for methylene blue removal, J. Polym. Environ. 29 (2021)1162-1175.https://doi.org/10.1007/s10924-020-01951-0

[56] W. Wei, L. Yang, WH. Zhong, SY. Li, J. Cui, ZG. WEI, Fast removal of methylene blue from aqueous solution by adsorption onto poorly crystalline hydroxyapatite nanoparticles, Digest J. Nanomater. Biostruct. 19 (2015) 1343-1363.

[57] K. Allam, A. El Bouari, B Belhorma, L. Bih, Removal of methylene blue from water using hydroxyapatite submitted to microwave irradiation, J. water resource prot. 8(2016) 358-371. 10.4236/jwarp.2016.83030

[58] A. Ragab, I. Ahmed, D. Bader. The removal of brilliant green dye from aqueous solution using nano Hydroxyapatite/Chitosan composite as a sorbent, Molecules 24 (2019) 847. https://doi.org/10.3390/molecules24050847.

[59] L. Fan, C. Luo, X. Li, F. Lu, H. Qiu, M. Sun, Fabrication of novel magnetic chitosan grafted with graphene oxide to enhance adsorption properties for methyl blue, J Hazard Mater 215 (2012) 272–279. https ://doi.org/10.1016/j.jhazm at.2012.02.068.

[60] W. Wang, Y. Zhao, H. Bai, T. Zhang, V. Ibarra-Galvan, S. Song, Methylene blue removal from water using the hydrogel beads of poly(vinyl alcohol)-sodium alginate-chitosan-montmorillonite, Carbohydr. Polym. 198 (2018) 518-528. https://doi.org/10.1016/j.carbpol.2018.06.124.

[61] A.H. Jawad, A.S. Abdulhameed, N.N. Bahrudin, N.N.M.F. Hum, S.N. Surip, S.S.A. Syed-Hassan, S. Sabar, Microporous activated carbon developed from KOH activated biomass waste: surface mechanistic study of methylene blue dye adsorption, Water Sci. Technol. 84 (2021) 1858-1872. https://doi.org/10.2166/wst.2021.355